Mass Spectrometry as a Preparative Tool for the Surface Science of Large Molecules

Stephan Rauschenbach,[1] Markus Ternes,[1] Ludger Harnau,[2] and Klaus Kern[1,3]

[1]Max-Planck-Institute for Solid State Research, D-70569 Stuttgart, Germany; email: s.rauschenbach@fkf.mpg.de

[2]70771 Leinfelden-Echterdingen, Germany

[3]Ecole Polytechnique Fédérale de Lausanne, CH-1015 Lausanne, Switzerland

Annu. Rev. Anal. Chem. 2016. 9:473–98

First published online as a Review in Advance on April 18, 2016

The *Annual Review of Analytical Chemistry* is online at anchem.annualreviews.org

This article's doi: 10.1146/annurev-anchem-071015-041633

Keywords

ion beam deposition, electrospray, preparative mass spectrometry, STM, STS, AFM

Abstract

Measuring and understanding the complexity that arises when nanostructures interact with their environment are one of the major current challenges of nanoscale science and technology. High-resolution microscopy methods such as scanning probe microscopy have the capacity to investigate nanoscale systems with ultimate precision, for which, however, atomic scale precise preparation methods of surface science are a necessity. Preparative mass spectrometry (pMS), defined as the controlled deposition of m/z filtered ion beams, with soft ionization sources links the world of large, biological molecules and surface science, enabling atomic scale chemical control of molecular deposition in ultrahigh vacuum (UHV). Here we explore the application of high-resolution scanning probe microscopy and spectroscopy to the characterization of structure and properties of large molecules. We introduce the fundamental principles of the combined experiments electrospray ion beam deposition and scanning tunneling microscopy. Examples for the deposition and investigation of single particles, for layer and film growth, and for the investigation of electronic properties of individual nonvolatile molecules show that state-of-the-art pMS technology provides a platform analog to thermal evaporation in conventional molecular beam epitaxy. Additionally, it offers additional, unique features due to the use of charged polyatomic particles. This new field is an enormous sandbox for novel molecular materials research and demands the development of advanced molecular ion beam technology.

INTRODUCTION

One of the most powerful paradigms of nanoscale science (1) is that the properties of a nanometer-sized object can be affected by the presence or absence of even a single atom. Hence, the current challenge of nanotechnology is to understand and control the vast complexity that arises when nanoscale objects interact with their environment. To master this problem, we need novel approaches that can comprehensively characterize the physical and chemical properties of nanoscale systems at atomic resolution. Required is nothing less than the precise knowledge of the atomic structure, including atomic positions as well as chemical information about each atom of a nanoscale object, such as a molecule.

Scanning probe microscopy (SPM) (2, 3) plays a central role in nanotechnology research because it enables researchers to observe atoms and molecules directly and even manipulate them individually (4, 5). Recording the mutual interaction of an atomically sharp tip with a surface, scanning probe microscopes map the surface, resolving subnanometer features or even single atoms (see **Figure 1*a*,*b***) (6, 7). The recorded quantity in scanning tunneling microscopy (STM) is the tunnel current or in atomic force microscopy (AFM) the frequency shift of an oscillating cantilever due to the exerted forces. The tunneling current in STM is related to the integrated local density of electronic states (LDOS) in the energy window between the applied bias and the Fermi energy. In AFM, the short-range forces from the attractive chemical bonding and the repulsive Pauli interaction decay at atomic length scale and are the origin of the atomic resolution topography, modulated by long-range Van der Waals and electrostatic forces (**Figure 1*c***) (8, 9).

In addition to imaging surfaces, SPM allows researchers to access the tip–surface interaction spectroscopically (**Figure 1*d*,*f***) (10). With the tip placed still over a specific location, a spectrum is recorded as a function of a parameter such as bias voltage (**Figure 1*d*,*f***), tip–surface distance, or oscillation amplitude (depending on the configuration of the setup, i.e., STM, AFM). These measurements reveal the local electronic structure (10) (**Figure 1*d*,*e***) or inelastic excitations such as bond vibrations (STM; **Figure 1*f***) (11), magnetic excitations (STM) (12, 13), or interaction potentials (AFM; **Figure 1*g***) (5). Combining spectroscopic and spatial information yields with atomic precision maps of physical properties, for example, density of states, chemical potential (**Figure 1*g***), work function (14, 15), surface charge (16), or orbital shape (**Figure 1*e***) (17), over a part of the surface.

Maximization of SPM performance relies strongly on the quality of the samples. Usually, only atomically flat crystal surfaces in ultrahigh vacuum (UHV) are suitable. Well-defined adsorbate films are prepared on these surfaces by vacuum evaporation of atoms or molecules. On such atomically defined samples, individual molecules can be investigated with spatial precision at the atomic level. The direct extraction of chemical information from SPM data, however, is almost impossible because the electronic states of neighboring atoms strongly interact.

Figure 1

Scanning probe microscopy. (*a*) Schematic of the principle of STM (scanning tunneling microscopy). (*b*) First atomic resolution image of a surface by STM [Si(111) 7 × 7]. Reproduced with permission from Reference 6. Copyright 1983 American Physical Society. (*c*) High-resolution, constant-height AFM image of a pentacene molecule using a CO-modified tip revealing the covalent bond structure. Reproduced with permission from Reference 18 and AAAS. (*d*) Local tunneling spectroscopy of C_{60} molecules shows molecular states (e.g., HOMO, LUMO). Adapted from Reference 19. (*e*) Experimental and theoretical density of states mapped at different energies for C_{60} (compare with panel *d*). Adapted from Reference 19. (*f*) Tunneling spectra of ethylene molecules reveal inelastic vibrational excitations, which distinguish the C-H bond from the C-D bond. Reproduced with permission from Reference 11 and AAAS. (*g*) Map of the potential depth of Co adsorption on a Cu(111) surface, derived by force spectroscopy. Adapted from Reference 5. Abbreviations: HOMO, highest occupied molecular orbital; LUMO, lowest unoccupied molecular orbital.

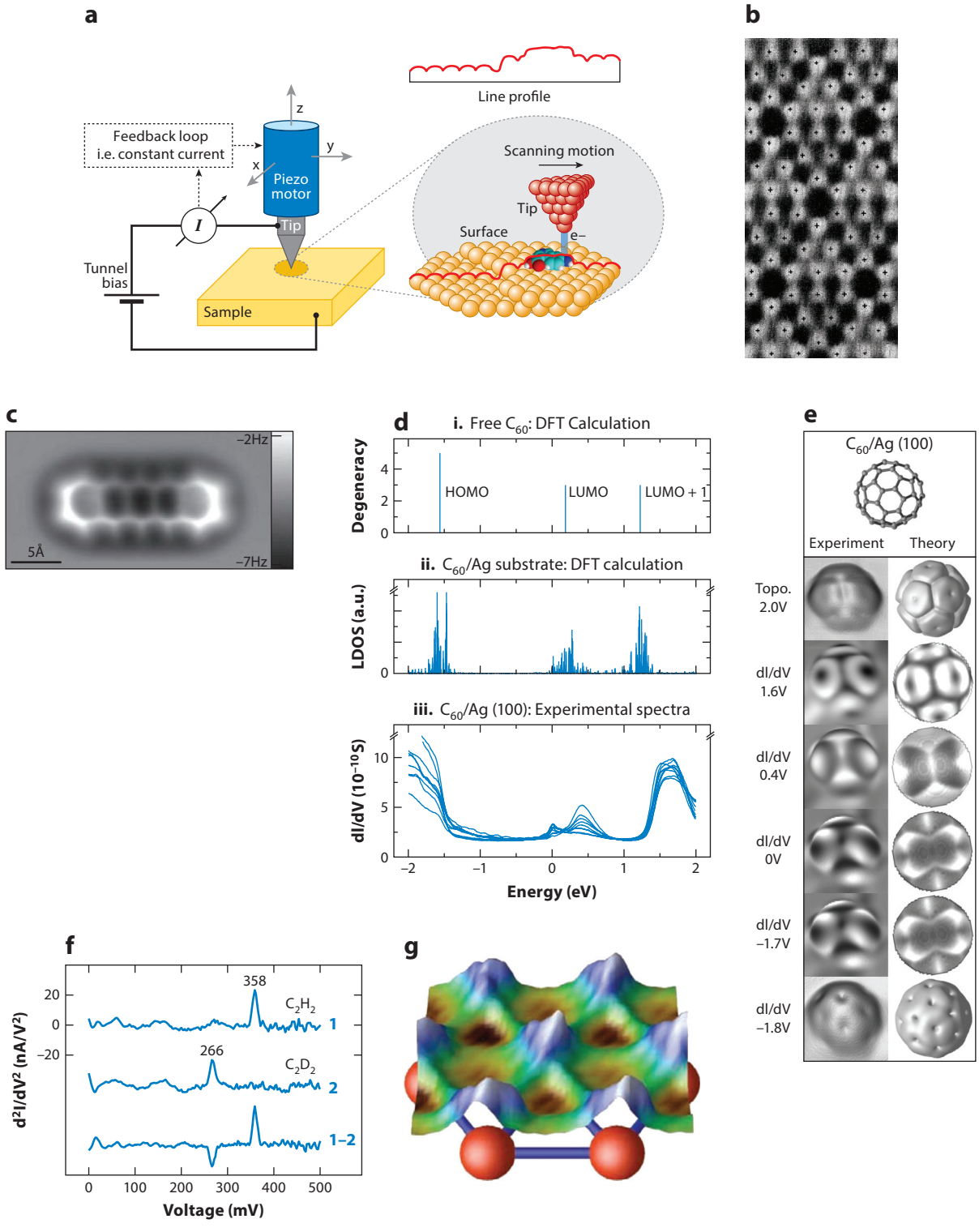
a
Line profile
Feedback loop
i.e. constant current
z
y
x
Piezo
motor
I
Tip
Tunnel
bias
Sample
Scanning motion
Tip
Surface
e–
b
c
–2Hz
5Å
–7Hz
d
i. Free C60: DFT Calculation
Degeneracy
4
2
0
HOMO
LUMO
LUMO + 1
ii. C60/Ag substrate: DFT calculation
LDOS (a.u.)
0
iii. C60/Ag (100): Experimental spectra
dI/dV (10–10S)
10
5
0
–2
–1
0
1
2
Energy (eV)
e
C60/Ag (100)
Experiment
Theory
Topo.
2.0V
dI/dV
1.6V
dI/dV
0.4V
dI/dV
0V
dI/dV
–1.7V
dI/dV
–1.8V
f
d2I/dV2 (nA/V2)
20
0
–20
358
C2H2
1
266
C2D2
2
1–2
0
100
200
300
400
500
Voltage (mV)
g

Mass spectroscopy (MS), in contrast, is the most powerful method to reveal the chemical composition of molecules. Mass spectrometers easily resolve a mass difference much lower than a single proton mass. In other words, MS reaches atomic precision in mass just like SPM is atomically precise in space. It entered the field of molecular nanoscience with the advent of soft ionization methods such as electrospray ionization (ESI) and matrix-assisted laser desorption ionization (MALDI), which made large, nonvolatile, organic, or biological molecules accessible as intact, molecular gas-phase ions (20–22).

Although it measures mass with extreme precision, even in a huge molecule, MS does not offer a direct route to molecular structure. Owing to the importance of structural information, mass spectrometers are often combined with structure-sensitive methods, typically targeting the gas-phase ion. Nearly every mass spectrometry application today includes either fragmentation (23) (collision-/surface-induced dissociation), hydrogen-deuterium exchange (24), ion mobility spectrometry (25), or covalent cross-linking (26). By these approaches molecular structure is in principle also investigated by atom-sized probes; however, the information provided can be rough, incomplete, or convoluted. Ion mobility spectrometry, for instance, measures the collision cross section, by which it is possible to distinguish differences at the atomic scale. The complex information of the three-dimensional (3D) molecular structure is thereby reduced to just one number, the collision cross section. Nevertheless, through systematic measurements combined with modeling, meaningful structural information can be extracted (27, 28).

A comparison of the strengths and weaknesses of mass spectrometry and SPM depicts them as complementary methods. With soft ionization sources even the largest biological molecules are available to MS for chemical characterization, whereas structural information is difficult to access. With SPM, the molecular structure can be imaged at atomic/subnanometer resolution, yet chemical composition remains obscured. In addition, SPM imaging of large, complex molecules, in particular biological molecules, is restricted by the condition of evaporability, which is needed to prepare chemically pure adsorbates on atomically defined metal surfaces in UHV.

Preparative mass spectrometry (pMS) presents itself as the perfect link between mass spectrometry and surface science experiments such as SPM by providing the well-defined, molecular ion beam of high chemical purity needed for UHV-grade sample preparation. pMS is the mass-selected deposition of (molecular) ions onto a surface. This definition also includes the terms ion soft landing/reactive landing or ion beam deposition (IBD), which are used synonymously. In principle, soft ionization sources can generate ion beams of large, nonvolatile molecules for any vacuum method, including vacuum deposition. Instead of being detected and generating the counts of a mass spectrum, an ion beam can simply be directed onto a surface in vacuum where the material is collected. Mass filters, as they are employed in a mass spectrometer, can be set to transmit only one ion species for deposition, preferable if they permit continuous beam operation. IBD thus inherits the advantage of chemical selectivity from MS and is therefore called preparative mass spectrometry.

The giant effort to enrich fissionable materials for the first nuclear explosions in the 1940s was the singular example of using pMS in the distant past of mass spectrometry's 100-year history (29). At that time this approach was too inefficient for other applications. For many years pMS received only little attention compared with mainstream analytical MS. With the emergence of biotechnology and nanotechnology and new gentle ionization sources for large molecules, pMS is being revisited because it bears great potential in two different, not mutually exclusive, applications: (*a*) As a fabrication method pMS can be used to grow films and modify surfaces, as it is extremely pure and specific, as well as offer a unique chemistry through ion–surface interactions. (*b*) As an analytical method pMS can serve as a sample preparation method for vacuum-based, high-performance surface science characterization methods such as SPM.

Surface modification by pMS is usually approached in combination with integral surface characterization methods, such as optical spectroscopy and mass spectrometry, both in situ and ex situ (30–34). pMS can be used for intact landing of polyatomic ions on surfaces (soft landing); inducing ion–surface reactions (reactive landing); and demonstrating effects such as elastic scattering, chemical scattering, or surface-induced dissociation. Further, the capacity of pMS for surface functionalization, for instance, dye attachment, catalytic activity, and enzyme immobilization, was developed.

These achievements show the potential of pMS as a novel synthesis and investigation method capable of using large, complex molecules. However, pMS also presents a challenge because both the deposition process and the resulting surface are highly complex. This challenge extends the original motivation to merge pMS with SPM because this combination allows researchers to inspect and understand the ion–surface interactions of complex molecules.

In the following section, we explore the potential of pMS as a means of vacuum deposition of large, nonvolatile molecules for high-resolution characterization by SPM. As a primer we show that pMS and SPM are an excellent match: Combined in one in situ UHV setup, they allow us to explore with unprecedented precision the world of large, functional molecules on surfaces. Thereafter, we review examples that illustrate the potential of the approach. (*a*) We show that pMS can serve as a tool equivalent to (organic) molecular beam epitaxy for submonolayer, monolayer, and thin film growth for nonvolatile molecules. (*b*) We discuss how the structure and conformation of large (biological) molecules can be controlled by IBD and investigated by SPM. (*c*) Finally, we show that SPM can access even the subtleties in the electronic structure of individual, highly complex molecules if the samples are prepared by pMS.

A BRIDGE BETWEEN WORLDS: PREPARATIVE MASS SPECTROMETRY WITH SOFT IONIZATION METHODS

Experimental Setup and Workflow

The typical electrospray–ion beam deposition/scanning probe microscopy (ES-IBD/SPM) experiment (sketched in **Figure 2**) combines two instruments and hence two workflows. The ion beam is prepared in the MS part (left side) of the setup, starting at ambient conditions required for ESI. A variety of ion optics guides the beam through the differentially pumped vacuum system to UHV, thereby defining and characterizing its properties. The substrate, an atomically defined crystal surface, is prepared and analyzed within a surface science experiment (right side) entirely performed in UHV. The actual deposition on the surface in UHV is the link between these two workflows.

The atomically defined (metal) surface is prepared by repeated cycles of sputtering (e.g., Ar^+ ions, 1 keV, 10 μA, 10 min) and annealing (approximately two-thirds of the melting temperature) a single crystal of well-defined orientation in UHV. The one given here is typical for metal surfaces. Each surface requires its own preparation protocol, especially procedures for semiconductor or insulator surface preparation, which may differ significantly. After the successful preparation is verified by SPM, the sample is transferred in situ to the deposition stage.

In parallel, the ion beam is generated by ESI and characterized by mass spectrometry and ion current measurements. pMS provides control over the deposition energy, the deposited ion species (molecule/fragment and charge state), and the deposition position. The ion species for deposition is selected by a mass-to-charge ratio (m/z) filter. The kinetic energy of the beam is determined typically by measuring deflection voltages in a retarding field geometry, which yields values for the kinetic energy per charge E_{kin}/z. The sample is biased (U_{sample}), either accelerating

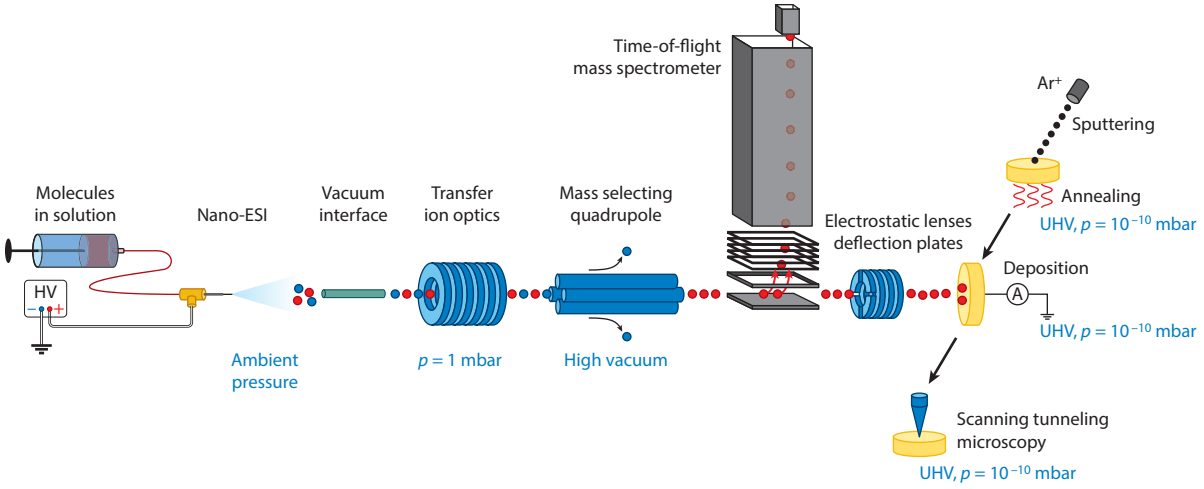

Figure 2

Scheme of an ES-IBD/SPM experiment. The ion beam is generated by ESI at ambient pressure (*left*) and transferred to UHV via a differentially pumped vacuum system (pressures given). The SPM sample is prepared under UHV conditions and is transferred in situ to a deposition stage and finally undergoes SPM analysis. Abbreviations: ESI, electrospray ionization; ES-IBD/SPM, electrospray ion beam deposition/scanning probe microscopy; UHV, ultrahigh vacuum.

or decelerating the ions, defining the deposition energy per charge as $E_d/z = E_{\text{kin}}/z - U_{\text{sample}}$. The beam is positioned on the surface by electrostatic lenses and deflection plates. The ion current on the sample is measured during deposition. Its integration, performed in real time during deposition, yields the deposited charge that can be converted to a molecular coverage for a known deposition area and ion charge state. By simply switching off the ion beam once a certain charge is reached, a desired coverage can be obtained with very high precision. After deposition, the sample is transferred in situ back to the SPM for the microscopy measurement.

The two workflows of SPM and pMS cross over only once in the deposition chamber of the ES-IBD instrument; however, an in situ UHV connection is required for contamination-free sample transfer. A rigid mechanical connection between ES-IBD and SPM typically inhibits the operation of both instruments at the same time, owing to the required mechanical stability of the environment for SPM. In particular, high-performance, low-temperature SPM measurements that involve tunneling spectroscopy can last several days, during which the operation of a pumping-intense, noisy ES-IBD source is impossible. Therefore, vacuum suitcases allow the transfer of samples between spatially separated, independent SPM and ES-IBD setups while maintaining UHV conditions during the entire transfer (35, 36).

Generally, ES-IBD setups closely resemble ESI mass spectrometers, which can be highly complex, expensive instruments containing ion optics such as lenses, ion guides, mass filters, and mass analyzers within a sophisticated, differentially pumped vacuum system (37–39). Some instrumentation approaches for ion deposition, however, reduce the amount of pumping stages or leave out ion optics elements to eliminate sources of ion loss or to reduce costs, at the expense of losses in functionality. Fewer differential pumping stages lead to higher pressure at the deposition position, which leads to contaminations unless only inert sample surfaces such as gold or graphite are used. Deposition setups can be operated without mass selection or mass analysis, which can lead to a partially or fully undefined surface, depending on the (unknown) contents of the beam (40).

Ion optics for collimation and focusing can be eliminated altogether (41). This approach in vacuum is called electrospray deposition (ESD). The ESD source skims the expanding ion/gas cloud that enters the vacuum through an unheated capillary and transmits its entire components without *m/z* selection or ion optics over three pumping stages to a surface in vacuum where a pressure of 10^{-7} mbar is measured during deposition. The simple design renders ESD a valuable deposition tool for SPM, however, with severe limitations. Inert surfaces such as Au(111) must be used and the deposited molecule should be unambiguously identifiable in STM in spite of potential contaminants (42). Yet even under such conditions the loss of the characteristic surface reconstruction on Au(111) surfaces (43), or adsorbate morphologies characteristic of the impact of large objects such as droplets or nanoparticles (44), indicates strong contamination and undefined surfaces after deposition.

The Need for Intense Ion Sources

Despite all the similarities, the decisive difference between ES-IBD and ES-MS lies in the beam intensity that is required for successful deposition and for a mass spectrum, respectively. Owing to the high sensitivity and very low background signal in a mass spectrometer, even a few hundred ions at the detector can make for a clear peak in the spectrum, whereas 100 molecules on a macroscopic sample surface area are almost impossible to find with an STM or to make an impact with respect to surface modification. For example, on a typical crystal surface area of 10 mm^2, 10^9 molecules have to be deposited to find one molecule per STM scan frame of, for instance, 100×100 nm^2. A monolayer of a large molecule occupying a surface area of 1 nm^2 (e.g., C_{60}, $m = 720$ u) on the same surface area requires 1×10^{13} molecules, which corresponds to a deposited charge of 444 pAh or 1.6 μC for singly charged ions.

Intense ion currents in the nanoampere range are the key requirement to achieve charges of this magnitude within a reasonable time frame on the order of 1 h. Nowadays, ion optics such as lenses, ion guides, and mass filters used in vacuo are very well optimized with respect to transmission. In particular, the introduction of a radio frequency (RF) ion funnel (45), which effectively collimates the ions entering the vacuum through the atmospheric interface into a usable ion beam, reduced the ion losses in vacuum such that they are minor compared with the losses in the atmospheric interface (46, 47).

Today, many ESI sources and vacuum interfaces lose more than 90% of the generated ions before they even enter the vacuum (48, 49). High transmission efficiency is demonstrated only for very low flow rates and very low solute concentrations, hence for low currents (50). Although ESI sources are a lively research topic (51–53), only a few reports on absolute current measurements are found in the literature because for MS applications the overall sensitivity and signal-to-noise ratio are more relevant than the absolute number of ions in the beam.

To improve the absolute ion current, pMS setups often use larger-diameter inlet capillaries and compensate for the increased gas load by higher pumping speeds (40, 46, 47). Leading experiments have demonstrated mass-filtered currents up to 10 nA in high vacuum (47) or 1.5 nA in UHV (with 6 nA in high vacuum) (46). However, even with ion currents in the high nanoampere range, ES-IBD is an academic tool, because technological coating applications require even higher fluences.

A milestone would be the coating of a silicon wafer-sized deposition target (≈100 cm^2) in reasonable time (<1 h) with one or several monolayers of molecules, for which microamperes of current are needed. A fundamental improvement of the vacuum interface is required to achieve this. Electrosprays in principle can generate microampere currents, and present ion optics provide good transmission characteristics. Simple upscaling of the present ion source's dimensions, however, is not a viable approach because the limit of available pumping power would be reached quickly. What

is missing from the development of highly efficient, intense ion sources is a deep understanding of ion transport in the vacuum interface, or more general, in fast-moving, compressible media. Simple hydrodynamic optimization by a funnel-shaped capillary inlet transmits currents up to 80 nA at unit transmission to the first pumping stage of the MS vacuum system, whereas the same interface with a conventionally designed inlet operated at only 10% transmission (46). This finding demonstrates that the precise quantification of losses caused by space charge, diffusion, and electric fields, combined with a rational approach toward optimizing gas flow, can lead to a much higher transmission efficiency and absolute ion current, ultimately leading ESI toward commercial coating applications.

FROM INDIVIDUAL MOLECULAR ADSORBATES TO THIN FILM GROWTH

The growth of nanostructures and crystalline layers from molecular beams begins with the adsorption of one particle, which then interacts with those that follow. The interplay of surface diffusivity of the adsorbates, their deposition rate, and the mutual interaction strength is critical to structure formation (1, 54, 55). SPM is ideal for studying nucleation, film morphology, and ordering because it allows investigators direct access to morphology and microscopic structure at the atomic level (54, 56). With a variable-temperature microscope the diffusion rate can be shifted to match the time constant of imaging. This allows the recording of frozen nonequilibrium structures at low temperature after deposition on a cold substrate, as well as the dynamics of structure formation when the sample is slowly warmed (57, 58).

Several pMS experiments have shown that molecular ions can be deposited on surfaces, that they remain intact under certain conditions, and that they even retain their charge (59). However, these studies have not investigated the structure and morphology of the deposited molecular film. The fundamental concept that nucleation and growth are determined by flux, diffusion, and mutual interaction may have to be altered or extended in consideration of the features specific to IBD. Charge retention can cause the adsorbates to interact repulsively and may add an additional time constant for the neutralization reaction to the description of the dynamics (60, 61). The dissipation of the energy from the hyperthermal surface collisions (62–65) may lead to transient mobility, defect generation, or chemical reactions.

Molecular Beam Epitaxy with Ions

Using a MALDI ion source in a modified magnetic sector mass spectrometer, Räder et al. (66) reported one of the first examples of ordered film growth from molecular ion beams (see **Figure 3*a***). The mass-selected deposition of phenalenes resulted in ordered layers of upright-standing π-stacked molecules on a graphite surface, which was imaged ex situ with AFM, resolving domains and molecular ordering. Laser ionization works well for polycyclic hydrocarbons, which, in addition to being nonvolatile, are often not even soluble. However, molecular ion sources based on pulsed lasers are not useful for deposition because they are neither intense nor do they provide a continuous beam. Therefore, ESI sources are currently preferred for molecular IBD and growth, because they generally produce higher and continuous currents.

All key features of conventional epitaxy, i.e., growth based on neutral-particle thermal evaporation, are documented for molecular IBD as well. Individual adsorbates are found at low coverage preferably at pinning sites and step edges, where they agglomerate into nucleation centers of few particles [see **Figure 3*b***, Mn_{12}–acetate$_{16}$ (Mn_{12}) on Au(111)]. Further growth leads to partially and, later, complete monolayer coverage films, which can be disordered (35, 36) (**Figure 3*b***) or ordered (67–71) (**Figure 3*a*,*d***). Depending on the mutual interactions between substrate and molecule,

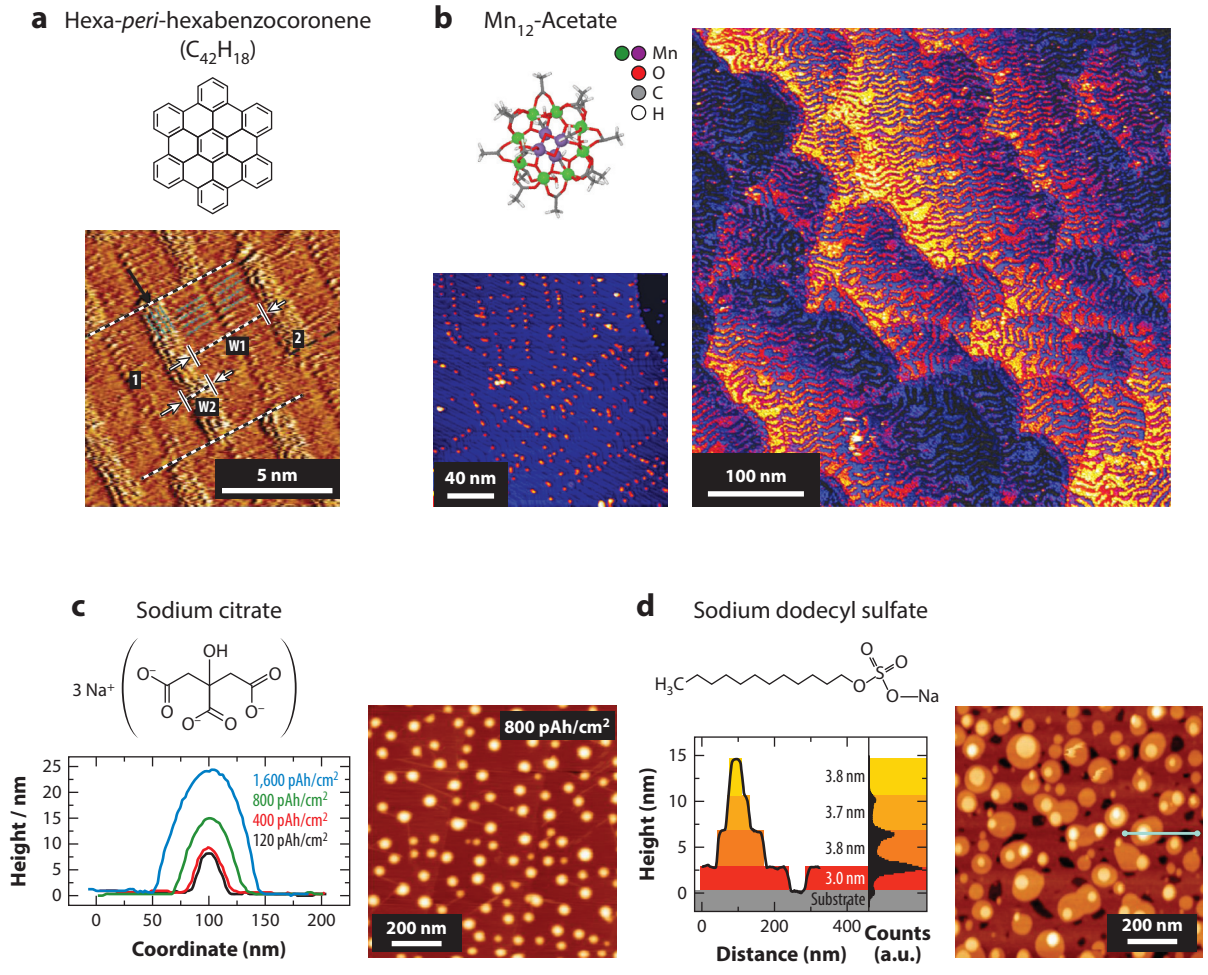

Figure 3

Growth by molecular ion beam deposition. (*a*) Films of soft-landed polycyclic aromatic hydrocarbons (hexa-*peri*-hexabenzocoronene) on graphite. Reproduced with permission from Reference 66. Copyright 2006 Macmillan Publishers Ltd: *Nat. Mater*. (*b*) High and low coverage of Mn_{12} on a Au(111) surface. Individual molecules, dimers, and trimers are found at the typical pinning sites, i.e., the elbow site of the reconstruction. Half monolayer homogeneous coverage of Mn_{12} preferably covering part of the Au(111) surface reconstruction. Reproduced from Reference 35. (*c*) Three-dimensional island growth of sodium citrate on a Si surface. (*d*) Two-dimensional layer growth of sodium dodecyl sulfate on a Si surface. Reproduced from Reference 67.

as well as on intermolecular interactions, multilayer coverage leads to films following a layer (**Figure 3*d***) or island growth mode (**Figure 3*c***). High-resolution SPM imaging further reveals epitaxial relationships between adsorbate (70) and substrate (67) or the substrate's surface reconstruction (35) (**Figure 3*b***) and well-defined grain boundaries between ordered domains (67, 71).

Hyperthermal Energy and Charge

Despite its close resemblance to MBE, molecular IBD epitaxy has additional features, i.e., hyperthermal impact energy and charged particles that lead to a number of new possibilities, questions,

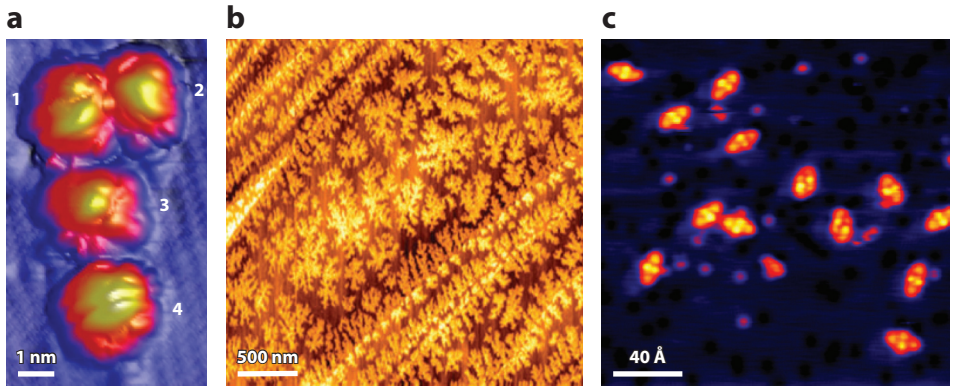

Figure 4

Reactive-landing molecular ion beam deposition. (*a*) The ruthenium dye N3 on an atomically resolved anatase surface binding via carboxy groups. Reproduced from Reference 36. (*b*) Deposition of mass-selected C_{58} buckyballs. In contrast to C_{60}, this fullerene species is reactive. Reproduced from Reference 72. (*c*) Na–crown ether complexes undergo a partial charge transfer. Reproduced from Reference 73.

and unusual observations. Reactive molecules that could otherwise not be thermally evaporated, such as the ruthenium dye N3 (**Figure 4*a***), can be brought into the gas phase by soft ionization methods such as ESI and deposited on a surface for reactive landing or soft landing (36). Reactive species can also be prepared in the gas phase, for instance, by ion-neutral collisions. The deposition of reactive C_{58} ions on graphite, derived by collisional fragmentation of C_{60} from an electron impact ion source, shows a strong intermolecular interaction evidenced by ramified island growth (**Figure 4*b***) (76).

IBD on insulating surfaces such as self-assembled monolayer-covered Au substrates has demonstrated charge retention (60, 61, 74). This observation suggests that the interactions of the charge of the impacting particles can influence growth just as flux or surface mobility can, which has so far not been studied systematically. However, revisiting some of the STM data—originally taken with ideas other than film growth—we find isolated molecules for which agglomerations due to intermolecular forces are expected, which hints at a repulsive interaction of the charge on the structure formation. For Mn_{12}–$acetate_{16}$ (Mn_{12}) on BN:Rh (111) (see **Figure 3*b***) (35) or Na–crown ether complexes on Cu(100) (73) (**Figure 4*c***) even crystallization is expected, because both species are highly mobile on the surface and do not offer strong binding sites that could limit diffusion (75). For the crown ether complex, density functional calculations indicate that the charge on the molecules is, at least partially, retained by the copper surface. Similarly, the charge on the Mn_{12} ion might be retained by the thin insulating boron nitride (BN) monolayer (76).

The assembly behavior of charged atoms and molecules at surfaces can be observed by STM. Although the interaction between two isolated like charges is repulsive, charges on a metal surface create upright-standing surface dipoles when screened by the free charge carriers in the metal. For like charges, the pure dipole–dipole interaction is repulsive, too. Additionally, indirect interactions, which are mediated by bulk electrons (77) or by surface-state electrons (78), generate an oscillatory, attractive, and repulsive interaction potential between the adsorbates, with the Fermi wavelength as the characteristic length and a decay of r^{-5} for bulk electrons and r^{-2} for surface-state electrons. Here, in particular, the long-range surface state interaction on the closed-packed hexagonal (110) facets of noble metals such as Au, Ag, and Cu, with a Fermi wavelength of several nanometers, can be utilized to create well-ordered lattices of only weakly bound molecules. This structure

formation has been observed for adsorbed atoms (79–81) and molecules (82, 83). Modulation of the electron density of states (84) or the Kosterlitz-Thouless phase transitions (85, 86) can be observed on these self-organizing structures.

Knowing that charge must be considered when discussing self-assembly of molecules on a surface, we may in turn learn about the fate of the charges, which is a key question for (low-energy) ion–surface interactions, from the analysis of self-assembled structures. Further, advanced SPM methods such as Kelvin probe force microscopy and scanning quantum dot SPM (87) can directly reveal even partial charges or the charge distribution of a molecule (88).

Surface-induced dissociation is an alternative to gas-phase fragmentation for mass spectrometry owing to its rich variety of interactions (89). This indicates that impact energy is an interesting candidate to influence film growth in IBD. With the kinetic energy still much higher than the kT value, even a soft-landing ion impact is expected to cause transient mobility of the deposited species. Both effects offer completely new possibilities for epitaxy: Surface-induced dissociation could be used to generate reactive species away from thermal equilibrium without heating that can undergo reactions that are otherwise not conceivable (89). A few examples demonstrate this possibility of covalent surface modification (64, 90–92). Whereas the energy dependence of the structure and the morphology of defects created by atomic ion impacts have been studied in depth (93, 94), little is known about the structures formed by energetic collisions of molecules because so far no high-resolution imaging has been performed. Nevertheless, the potential of covalent modification at room temperature in a clean vacuum environment is of importance for fragile functional surfaces or demanding device integrations. Similarly, enhanced mobility may support crystalline growth without thermally straining fragile functional molecules. STM imaging recently showed that the secondary structure of a macromolecular ion can be influenced by charge state and deposition energy (see **Figure 5**); however, an effect on crystalline growth has not yet been shown.

STRUCTURAL CHARACTERIZATION OF COMPLEX BIOLOGICAL MOLECULES

The 3D structure of biological molecules, specifically proteins, is directly connected to their function. Precise structural characterization therefore is of utmost importance. As a sample preparation method, ES-IBD yields well-defined surfaces that can be imaged by UHV-STM, which in principle offers spatial resolution at the atomic level. Applying this approach to biological molecules, we are confronted with the following questions: What spatial resolution can be achieved? Is the primary, secondary, or tertiary structure of biological molecules influenced by the landing process? What information about biological or synthetic macromolecules can be extracted from an SPM image?

One of the first IBD experiments to use gentle electrospray ionization demonstrated the intact soft-landing deposition of protein ions of low kinetic energy via the detection of molecules in the washing solution (95). When enzymatic activity on the prepared protein microarrays was found, the same experiment hinted that the native conformation was retained. Similarly, infrared spectroscopy (96) detected the retention of helical conformations of peptides after soft-landing deposition. These successful depositions indicate the feasibility of imaging the 3D conformation of immobilized proteins or peptides prepared by pMS. Other early experiments showed that soft surfaces (38, 59, 97) or even liquid surfaces (98) are advantageous for soft-landing deposition and conformation retention of the 3D structure.

Controlling Protein Conformation on the Surface

In contrast to vapor deposition, pMS inherits from mass spectrometry the precise control of the molecular beam with respect to content, charge state, and kinetic energy. Ion mobility/mass

Figure 5

Controlling the protein conformation of cytochrome *c* (CytC) by electrospray ion beam deposition. (*a*) Soft landing of folded proteins achieved by gentle electrospray ionization, avoiding denaturing condition such as organic solvent or low pH. (*b*) High-charge states of CytC immobilized on a Cu(100) surface in an extended conformation. (*c*) Low-charge state CytC on a Cu(100) surface yields a compact conformation. (*d*) High-charge-state CytC on a Au(111) surface yields compact conformation after freezing out diffusion by cooling to 40K. (*e*) Persistence length of CytC as a function of landing energy. Higher deposition energy leads to a more compact conformation. Panels *a* and *d* are reproduced from Reference 103. Panels *b*, *c*, and *e* are reproduced from Reference 65.

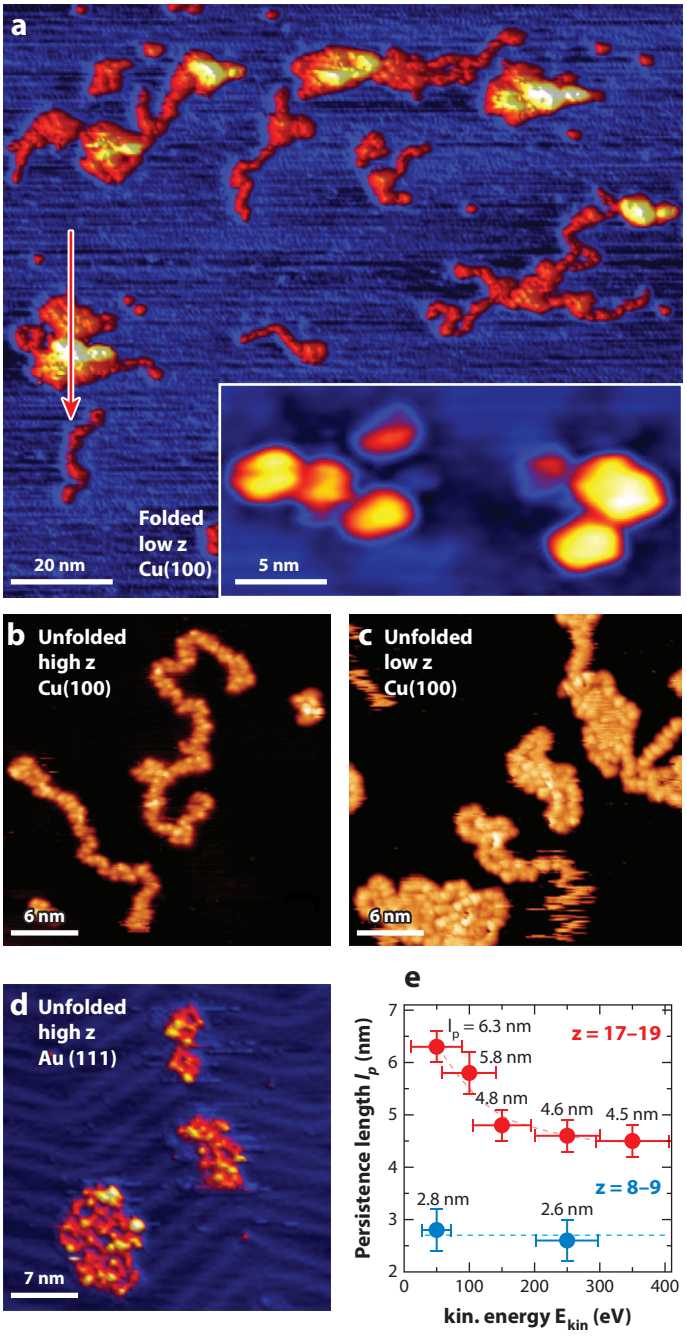

spectrometry measurements of various proteins demonstrated that this also implies control over the conformational state in the gas phase (25, 99–102).

To demonstrate the applicability of this control scheme, atomically flat metal surfaces were coated with protein ion beams, systematically varying the deposition parameters, and afterward imaged by STM (65, 103). Many deposition parameters were found to directly influence the adsorption conformation of the proteins on the surface (summarized in **Figure 5** for the case of cytochrome *c*).

A native conformation or an unfolded conformation of the protein can be selected by electrospray and solution conditions (99, 103). Solutions of neutral pH without organic solvent contain native proteins and yield low-charge-state ion beams, whereas unfolded proteins from acidic solutions with organic solvent yield high-charge-state ion beams. Conformation selection by solvent is further supported by *m/z* selection of high- or low-charge states. The difference between folded and unfolded proteins is directly visible in the STM micrographs. Folded proteins appear as globular features that are several nanometers in height and diameter (**Figure 5*a***), and unfolded proteins are imaged as extended strands (**Figure 5*b***), which are sometimes backfolded in two dimensions (**Figure 5*c,d***). Because the molecule–surface interaction on metal surfaces is strong, the deposition of unfolded proteins always leads to 2D structures. Thus, any 3D structure can stem only from the, at least partial, retention of the native conformation of the 3D protein after deposition.

STM imaging of 2D adsorbed, unfolded strands shows submolecular details, whereas the 3D proteins are imaged as one large protrusion. The resolution of SPM imaging critically depends on the shape and stability of the tip. For high-aspect-ratio structures like a globular protein, a similarly large, high-aspect-ratio tip has to be well-defined and stable to yield good-quality imaging, which is rather unlikely. Molecular functionalized STM or AFM tips (104–106) may further improve the resolution. In addition, methods that provide true 3D imaging, such as electron holography (107) or free-electron laser X-ray scattering (108), might soon reach a resolution similar to that of STM. Moreover, combining these methods with pMS might be advantageous. In all cases, the interpretation of the acquired images crucially depends on well-defined deposition of a well-known folded species.

Three experimental parameters of ES-IBD can be used independently to define the 2D conformations of unfolded proteins: surface mobility, ion charge state, and deposition energy. On strongly interacting surfaces such as Cu(100), the thermal diffusion of the unfolded proteins is inhibited. When the protein is fully immobilized at room temperature, extended, random 2D conformations are observed. On less strongly interacting surfaces such as Au(111), the proteins are mobile and their conformations change due to diffusion, which leads to self-interaction. Therefore, at low temperatures (e.g., 40K) the protein eventually finds a stable, local energy minimum. Observed conformations are compact, yet no uniform shape is recognizable, possibly indicative of a randomly folded conformation (**Figure 5*d***).

The gas-phase charge state defines the mechanical stiffness of the polypeptide and is related to either a compact or an extended gas-phase conformation for high- or low-charge states, respectively. On a surface at inhibited diffusion, e.g., Cu(100), the effect of the stiffness and gas-phase conformation on the deposition can be directly observed by STM. Upon impact, the kinetic energy acts to compact the polymer, which is resisting with its stiffness. Stiff, high-charge-state proteins are less deformed, which results in extended conformations (**Figure 5*b***), whereas soft, low-charge states lead to compact, 2D-folded conformations (**Figure 5*c***).

When the deposition energy is varied, it becomes evident that the interplay of stiffness and gas-phase conformation defines the adsorption conformation. **Figure 5*e*** shows the evolution of the persistence length, i.e., the length at which the polymer is approximately straight, with the deposition energy for high- and low-charge-state protein ions. With higher deposition energy the

adsorption conformation of stiff, high-charge-state proteins becomes more compact, whereas the soft, low-charge-state proteins already have a compact adsorption conformation at low deposition energy and thus their persistence length does not further decrease (65).

For the short time span of the collision event, from initial touch until the kinetic energy has dissipated, parts of the polypeptide chain are mobile even without thermal diffusion. Compact 2D conformations could also be attained by this transient mobility, which would result in compact 2D patches similar to the structures formed by thermal diffusion (compare **Figure 5*c*** with **5*d***).

For a protein such as cytochrome *c*, which is folded in solution, a single recurring folded structure in vacuum on a metal surface cannot be expected. However, polypeptide chains rationally folding on surfaces might exist, but they have their own unique sequences that are different from those of proteins that fold in solution. These sequences are not yet known to us, but the deposition of biological or other sequence-controlled polymers (109) could be a promising approach to fabricate complex, surface-based, molecular nanostructures via self-assembly. Such an approach would inherit the successful mechanisms of biological molecules, for instance, sequence-encoded structures (110) from folding and functionality by induced-fit molecular recognition (111). A reduction of complexity, i.e., the study of small polypeptides, is a promising starting point for this goal as well. Indeed, researchers have recently used STM and computer simulations to investigate the formation of stable molecular nanostructures via 2D folding of the nine-amino-acid peptide bradykinin (112) and the sequence-controlled self-assembly of angiotensin peptides (71).

Modeling the Deposition of Macromolecules

The conformation of macromolecules deposited on substrates depends on their kinetic energy and on the number and location of the charges on the polyions. Atomistic simulations, typically from density function theory (DFT) but also from molecular dynamics (MD), are very helpful for interpreting high-resolution STM data. Models encompassing the size of most macromolecules used in ES-IBD, however, cannot be tackled by DFT due to their size. Similarly, they present a real challenge to MD simulations, because very long simulations from a variety of adsorption geometries are needed to understand the adsorption process at the atomic length scale (113).

The relevance and potential of theoretical modeling of deposition are illustrated by MD simulations of the charged protein cytochrome *c* (CytC) deposited on metal surfaces. The simulations show that the end-to-end distance of the unfolded protein increases as the kinetic energy decreases, because more time is available for molecular reorientations after a part of a protein first contacts the metal surface (65). Representative protein conformations of highly charged CytC (valence $z = 18$) following collisions with a Cu(100) surface are shown in **Figure 6**. The unfolded protein exhibits an extended shape similar to a linear polymer and is partly aligned by the external electric field such that it touches the copper surface first with atoms located close to one of its ends. The initial kinetic energy of the protein is lower during deposition shown in **Figure 6*a–d*** than during deposition shown in **Figure 6*e–h***. As a result, the protein with low kinetic energy has sufficient time to adopt a stretched conformation, characteristic of highly charged CytC (**Figure 6*d***). In contrast, faster deposition leads to a less extended conformation for the protein with high kinetic energy (**Figure 6*h***) because both ends of the protein are immobilized during the intermediate states of deposition (**Figure 6*g***).

These numerical results together with the corresponding experimental data (65) (see **Figure 5**) indicate that the conformation of macromolecules deposited on substrates can be controlled by adjusting their kinetic energy. Future work may focus on understanding how extended proteins are oriented on metal surfaces in order to design orientationally ordered, i.e., 2D nematic, macromolecular coatings. To this end, one may consider surfaces of low symmetry, such as

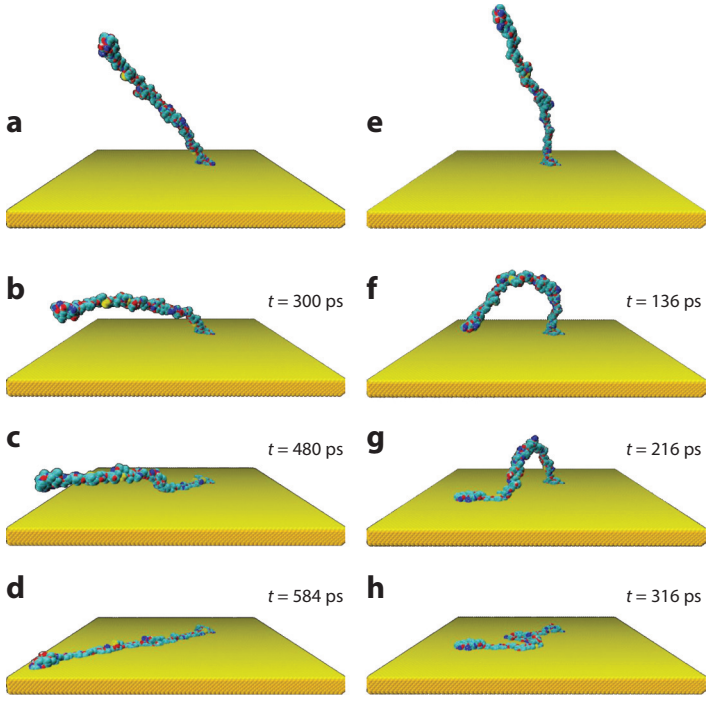

Figure 6

Snapshots of the unfolded protein cytochrome *c* obtained from molecular dynamics simulations of deposition on a Cu(100) surface for low (*a–d*), high (*e–h*), and initial kinetic energy. In panels *a* and *e* both proteins initially touch the surface, with atoms located close to one of their ends. During the subsequent slow deposition in panels *b*, *c*, and *d*, the protein has sufficient time to adopt a stretched conformation. The final conformation of the protein in panel *h* is less extended than it is in panel *d* because both ends of the protein are immobilized during the intermediate states of fast deposition in panel *g*. The time *t* is measured with respect to the states in panels *a* and *e*.

Cu(110), which promote orientational ordering of adsorbed macromolecules owing to a template of atomic rows characteristic of this facet (114). In addition, varying the orientation of the substrate with respect to the ion beam to align the macromolecules before collision with the substrate should be possible but has not been tested for protein ion beams (115).

High-Resolution Imaging of Macromolecules

Understanding the structure–function relationship and self-assembly of large molecules is critically dependent on precise knowledge of their atomic structure, be it in solution or in vacuum at a surface. The capability of STM to image large molecular objects at high resolution and to identify their building blocks has been demonstrated, for instance, for single-strand DNA (ssDNA) (115) (**Figure 7*c***) and large porphyrin nanorings (42) (**Figure 7*b***). In both cases the molecules were nonvolatile and had to be brought onto the surface with a method alternative to evaporation. For ssDNA a pulsed liquid inlet was used, and the porphyrin nanorings were deposited by ESD (42).

Comparing these results to the image of a large unfolded protein deposited by ES-IBD [bovine serum albumin, BSA, on a Cu(100) surface; **Figure 7*a***], we find that all three molecules are imaged at similar submolecular/subnanometer resolution. Their structural elements, which are

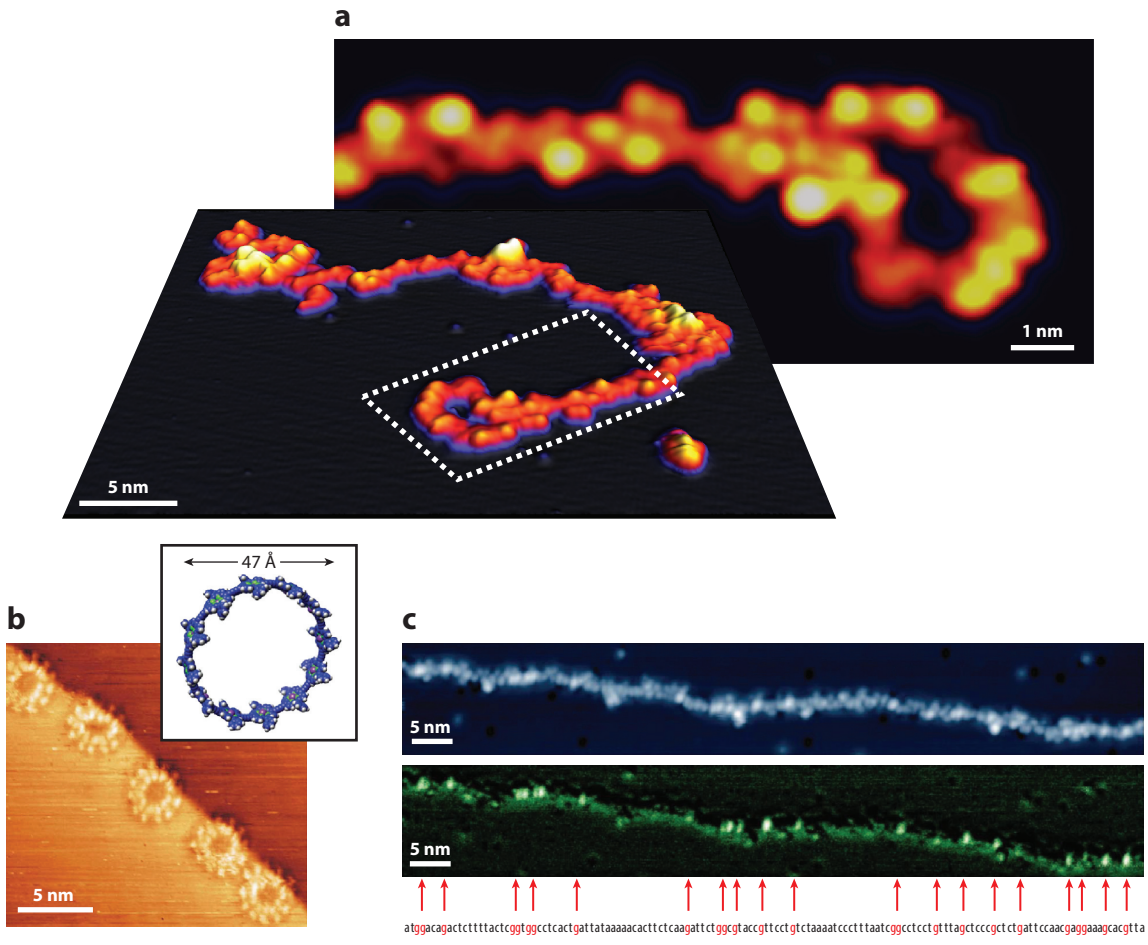

Figure 7

Resolution achieved by STM imaging of macromolecules. (*a*) Unfolded BSA strand on a Cu(100) surface showing features at amino acid resolution. Adapted from Reference 103. (*b*) A large macrocyclic ring of 12 porphyrin monomers deposited by ESD. The STM image shows one feature per porphyrin. Reproduced with permission from Reference 42. Copyright 2011 Macmillan Publishers Ltd: *Nature*. (*c*) Partial sequencing of single-stranded DNA deposited through a pulsed inlet. Adapted from Reference 115. The lower panel highlights the guanine bases. Abbreviations: BSA, bovine serum albumin; ESD, electrospray deposition; STM, scanning tunneling microscopy.

the individual porphyrin units, the nucleic bases, or the amino acids, respectively, are mapped as distinguishable features. The number and symmetry of the features of the nanoring clearly relate them to the porphyrin subunits. The DNA strand shows distinctly bright features. In an experiment with a known reference sequence, those features have been related to the guanine residues of the DNA.

The unfolded strand of BSA, a protein of several hundred amino acids, shows individual protrusions one amino acid in length. Hence, the vast majority of the sequence is resolved (103). However, a complete characterization of this protein, which ultimately includes the chemical identification of the residues, is not directly possible from the STM imaging data. In contrast to the porphyrin rings, proteins do not have a high symmetry that allows their features to be clearly identified. Also, an unambiguously distinguishable feature like the one presented by the DNA has not been found.

This is not merely coincidence: DNA is designed by nature to store information redundantly and make it accessible. Its glycophosphate backbone is stiff and neatly separates only four different nucleic bases, such that they interact with the surface without additional interference. Hence, the same nucleic bases reproduce the same adsorption conformation and thus identical LDOS.

In contrast, proteins are more chemically diverse than DNA. Their sequences are connected via a compact, flexible polypeptide backbone made for folding and mutual interaction, not for information storage and transfer. Thus, additional symmetry or chemical information, which could support the identification of the protein residues in the STM images, is not available. Even though it is possible to prepare an unfolded protein on the surface in a fully extended conformation by selecting high-charge states for deposition, it is likely that the same amino acids along the chain will find themselves in different environments due to self-interaction with neighboring residues and different distances and orientations toward the substrate. This results in different adsorption conformations and hence different contrast due either to different LDOS or to height. Tunneling spectroscopy or imaging with modified AFM tips (104–106, 116, 117) could add additional information to the image, enabling investigators to extract chemical information, as outlined in the next section. To this aim, however, again the reduction of complexity, i.e., the investigation of short polypeptides of well-defined sequences, is the better starting point (71).

INVESTIGATING ELECTRONIC AND MECHANICAL PROPERTIES OF MOLECULES

One of the most fascinating strengths of SPM is that it can detect physical and chemical properties at the submolecular level by performing spectroscopic measurements. In this context, bias spectroscopy with a scanning tunneling microscope is the most commonly used spectroscopic method, in which the differential junction conductance dI/dV versus the applied bias voltage V is recorded while the probing tip rests statically over the point of interest. The differential conductance directly measures the tunneling probability at the applied bias and is proportional to the convolution of the energy-resolved LDOS in the tip and the sample (118, 119). By characterizing the tip's LDOS, this method directly accesses such fundamental properties as the energy of molecular orbitals and their hybridization with underlying substrate electrons.

Additionally, tunneling electrons with sufficient energy can locally probe vibronic or magnetic excitations on the surface or in adsorbate atoms and molecules. When inelastic channels open at the bias voltage, the increased tunneling probability corresponding to the energy of the excitation leaves characteristic, usually bias-symmetric steps in the dI/dV or equivalent peak-dip structures in the second derivative of the current (d^2I/d^2V) (120, 121). At low temperatures the energy resolution is sufficient to distinguish between different isotopes in molecules due to the shift in bond vibration with atomic mass (120, 122, 123).

Since the advent of SPM, many other spectroscopy methods have been employed to locally resolve, for example, the apparent barrier height by measuring the current decay versus tip–sample separation (124) or to determine lifetimes of excitations by pump-probe methods (125–127). Here, noncontact AFM, with its access to the forces acting between the tip and the sample, dramatically extends the spectroscopic possibilities: The atomic scale interaction potentials are measured directly (5, 128) when force-distance curves are integrated; local Kelvin probe force spectroscopy is performed, or surface charges are directly mapped (117), when the interacting forces are minimized with an applied bias. The capabilities of ES-IBD allow one to use local spectroscopy on individual, large, nonvolatile molecules. However, at present this combination has been applied in only a few instances, representing the forefront in this research area.

Figure 8*a*,*b* show STM images of ruthenium-based N3 dye molecules on the Au(111) surface and on the technologically relevant TiO_2–anatase surface, respectively, after ES-IBD preparation

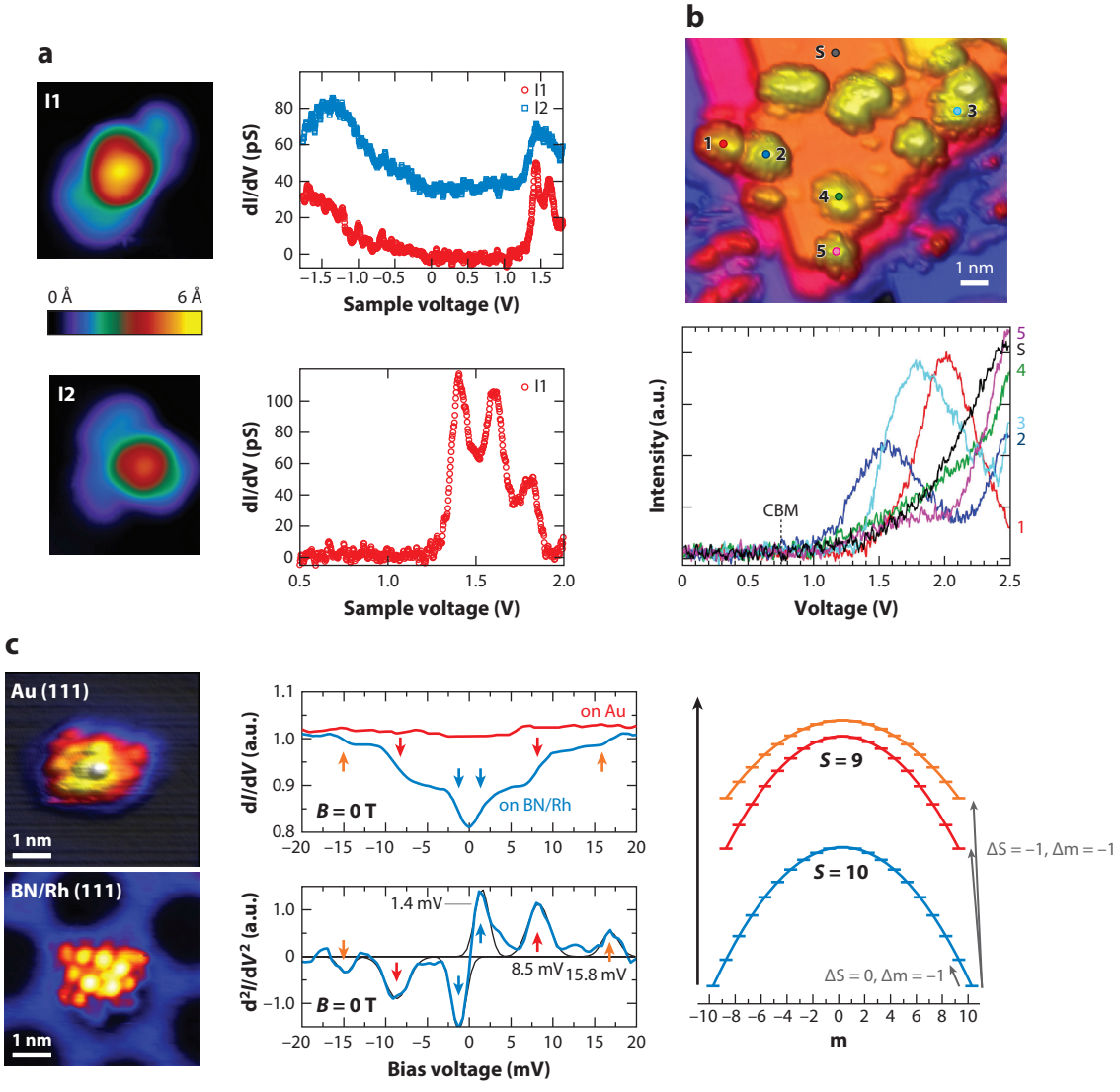

Figure 8

Examples of STS measurements on ES-IBD-grafted molecules on surfaces. (*a*) Topographic images (*left*) and STS data (*right*) of the ruthenium-based dye N3 on a Au(111) surface. Image sizes are 4×4 nm^2 for I1 and 4×3.3 nm^2 for I2. Reproduced with permission from Reference 129. Copyright 2013 American Chemical Society. (*b*) The same N3 dye molecule deposited on a TiO_2 surface shows strongly adsorption-dependent spectroscopic features. Figures adapted from Reference 36. (*c*) Images of individual Mn_{12}–acetate$_{16}$ molecules adsorbed on a Au(111) surface and on the monoatomic *h*-BN/Rh(111) surface. STS at low temperatures ($T = 1.5$K) reveals a quenched magnetic moment for molecules on the Au(111) surface, but bias-symmetric steps on the BN/Rh(111) surface because of magnetic excitations. Figures adapted from Reference 35. Abbreviations: ES-IBD, electrospray ion beam deposition; STS, scanning tunneling spectroscopy.

(129, 130). These molecules are widely used in dye-sensitized solar cells; however, within a solar cell, accessing the electronic properties of individual dye molecules is impossible. In both examples scanning tunneling spectroscopy (STS) is used to clarify how the dye molecule binds to the surface. For Au (**Figure 8*a***), the most likely case is the Au-S bond, which is confirmed by observations of equally spaced replicas of the lowest unoccupied molecular orbital (LUMO) due to resonant tunneling into vibronic states. STM detects multiconformational binding on the anatase surface (**Figure 8*b***). These different adsorption geometries strongly influence the position of the LUMO level as directly seen in the widespread onset of bands in STS.

Figure 8*c* show Mn_{12}–$acetate_{16}$ molecules, an archetypical molecular magnet with high intrinsic spin and long spin-relaxation times (131), adsorbed on Au(111) and *h*-BN:Rh(111) surfaces. Observations of the characteristic shape of the molecule reveal the power of pMS, which permits the preparation of this infamously fragile molecule (132). However, in the STM topography the molecule appears to be intact on both substrates, whereas STS reveals that the molecule loses its magnetic properties only on the Au surface due to the hybridization of the molecular states with the metal (133). By contrast, low-energy excitations on the ultrathin decoupling layer *h*-BN:Rh(111) are observed. By calculating the spin-flip transition probabilities (134) of this complexly coupled system with a ground state total spin of $S = 10$, one can identify the observed transitions as one excitation at low energy, which changes only the magnetic quantum number, and two excitations at higher energy, which additionally change the total spin from $S = 10$ to $S = 9$, demonstrating an intact magnetic core (35).

This experiment is only possible in a low-temperature scanning tunneling microscope using pMS for preparation and a vacuum suitcase for linking the two instruments. This experiment marked the first time a molecular magnet was accessed as an individual molecule on a surface, which perfectly underlines the relevance of pMS combined with SPM. Extrapolating the developments in synthetic chemistry and molecular nanoscience leads to applications to even larger, multifunctional molecules or biomimetic systems such as sequence-controlled polymers. In these systems, locally addressing functions and relating them to structure, while maintaining chemical control over the environment, for which local probe spectroscopy may be a crucial tool, will be extremely important.

CONCLUSION AND OUTLOOK

The preparation of ultrapure, atomically defined surfaces is a new application of pMS that has great prospects. In principle, the well-defined preparation of a sample is useful for any (surface science) characterization method. It is thus not surprising that pMS was successfully used in combination with many other surface analysis methods such as secondary ionization mass spectrometry (63, 135), infrared spectroscopy (96), Raman spectroscopy (64, 136), and electrochemistry (92).

Nevertheless, we think that SPM has a special role because it can fully exploit the high degree of control and purity that pMS offers. In addition, the current challenges of molecular nanotechnology seem tailor-made for the range of molecules available via electrospray ionization. The chemical selectivity from mass spectrometry and the high spatial resolution of SPM allow for complexity without losing atomic precision, opening the road to investigations of individual macromolecules or molecular coatings.

A highly detailed view of molecular structure, conformation, and even dynamics is now possible. This perspective is significant for fundamental research, especially for biological model systems, e.g., proteins, peptides, or glycans, or model systems of synthetic origin. Certainly, the interactions on a surface in vacuum will be different from those in an aqueous environment, which is particularly relevant for biology. Nevertheless, the complexity of the interactions prevails and fundamental

aspects such as folding or sequence-controlled assembly seem feasible in vacuum as well. In fact, surface-based studies in vacuum do not exclude the possibility of investigating the role of solvents at the molecular scale (137). Furthermore, the chemistry of ions at the surface, especially in collisions at hyperthermal energy, are worthy of investigation, both from chemical and morphological points of view (37, 138).

Whether pMS will be of widespread commercial use depends on the availability of intense ion sources. The pMS community is already heavily invested in the development of innovative MS equipment, often with the aim of higher intensity and efficiency (46, 47, 53). However, these sources will be developed only if applications are in sight. Functional coatings fabricated by pMS have been demonstrated (74, 139), and IBD can be used to fabricate device surfaces under conditions accessible only to hyperthermal ion beams (36, 64).

Very few ES-IBD/SPM systems are in operation (39, 140), but several new systems are under development. pMS could be of great importance to other surface science analysis instruments such as synchrotron sources (141) or electron microscopes (107, 108). Standardized commercial solutions for pMS/SPM do not exist and are not likely to appear in the near future. Devising and operating both MS and SPM equipment, which is rare in combination and further limits demand, require a highly specialized laboratory or vendor. Moreover, although the combination of SPM and pMS has the potential to be instrumental in the development of nanotechnology applications, SPM will not be part of a pMS setup focusing on high-productivity, thin film fabrication.

Currently, the scanning probe community continues to advance by measuring new physical effects with even higher precision, encompassing the highest energy resolution at milli-Kelvin temperatures (142), by using superconducting tips, or by introducing pump-probe schemes to access fast dynamics (125). Hence, present pMS/SPM experiments have only scratched the surface of the potential resting in this powerful combination.

DISCLOSURE STATEMENT

The authors are not aware of any affiliations, memberships, funding, or financial holdings that might be perceived as affecting the objectivity of this review.

LITERATURE CITED

1. Barth JV, Costantini G, Kern K. 2005. Engineering atomic and molecular nanostructures at surfaces. *Nature* 437:671–79
2. Binnig G, Quate CF, Gerber CH. 1986. Atomic force microscope. *Phys. Rev. Lett.* 56:930–33
3. Binnig G, Rohrer H. 1987. Scanning tunneling microscopy-from birth to adolescence. *Rev. Model. Phys.* 59:615–25
4. Stroscio JA, Eigler DM. 1991. Atomic and molecular manipulation with the scanning tunneling microscope. *Science* 254:1319–26
5. Ternes M, Lutz CP, Hirjibehedin CF, Giessibl FJ, Heinrich AJ. 2008. The force needed to move an atom on a surface. *Science* 319:1066–69
6. Binnig G, Rohrer H, Gerber CH, Weibel E. 1983. 7×7 Reconstruction on Si(111) resolved in real space. *Phys. Rev. Lett.* 50:120–23
7. Giessibl FJ. 1995. Atomic resolution of the silicon (111)-(7×7) surface by atomic force microscopy. *Science* 267:68–71
8. Tersoff J, Hamann DR. 1983. Theory and application for the scanning tunneling microscope. *Phys. Rev. Lett.* 50(25):1998
9. Giessibl FJ. 2003. Advances in atomic force microscopy. *Rev. Model. Phys.* 75:949–83
10. Zandvliet HJW, van Houselt A. 2009. Scanning tunneling spectroscopy. *Annu. Rev. Anal. Chem.* 2:37–55

11. Stipe BC, Rezaei MA, Ho W. 1998. Single-molecule vibrational spectroscopy and microscopy. *Science* 280:1732–35
12. Hirjibehedin CF, Lutz CP, Heinrich AJ. 2006. Spin coupling in engineered atomic structures. *Science* 312(5776):1021–24
13. Hirjibehedin CF, Lin C-Y, Otte AF, Ternes M, Lutz CP, et al. 2007. Large magnetic anisotropy of a single atomic spin embedded in a surface molecular network. *Science* 317(5842):1199–203
14. Vitali L, Levita G, Ohmann R, Comisso A, De Vita A, Kern K. 2010. Portrait of the potential barrier at metal-organic nanocontacts. *Nat. Mater.* 9(4):320–23
15. Della Pia A, Riello M, Floris A, Stassen D, Jones TS, et al. 2014. Anomalous coarsening driven by reversible charge transfer at metal–organic interfaces. *ACS Nano* 8(12):12356–64
16. Mohn F, Gross L, Moll N, Meyer G. 2012. Imaging the charge distribution within a single molecule. *Nat. Nanotechnol.* 7:227–31
17. Gross L, Moll N, Mohn F, Curioni A, Meyer G, et al. 2011. High-resolution molecular orbital imaging using a *p*-wave STM tip. *Phys. Rev. Lett.* 107:086101
18. Gross L, Mohn F, Moll N, Liljeroth P, Meyer G. 2009. The chemical structure of a molecule resolved by atomic force microscopy. *Science* 325:1110–14
19. Lu X, Grobis M, Khoo KH, Louie SG, Crommie MF. 2003. Spatially mapping the spectral density of a single C_{60} molecule. *Phys. Rev. Lett.* 90:096802
20. Dole M, Mack LL, Hines RL, Mobley RC, Ferguson LD, Alice MB. 1968. Molecular beams of macroions. *J. Chem. Phys.* 49:2240
21. Karas M, Bachmann D, Hillenkamp F. 1985. Influence of the wavelength in high-irradiance ultraviolet laser desorption mass spectrometry of organic molecules. *Anal. Chem.* 57(14):2935–39
22. Fenn JB, Mann M, Meng CK, Wong SF, Whitehouse CM. 1989. Electrospray ionization for mass spectrometry of large biomolecules. *Science* 246(4926):64–71
23. Dongre AR, Somogyi A, Wysocki VH. 1996. Surface-induced dissociation: an effective tool to probe structure, energetics and fragmentation mechanisms of protonated peptides. *J. Mass Spectrom.* 31(4):339–50
24. Englander SW. 2006. Hydrogen exchange and mass spectrometry: a historical perspective. *J. Am. Soc. Mass Spectrom.* 17(11):1481–89
25. Bohrer BC, Merenbloom SI, Koeniger SL, Hilderbrand AE, Clemmer DE. 2008. Biomolecule analysis by ion mobility spectrometry. *Annu. Rev. Anal. Chem.* 1:293–327
26. Petrotchenko EV, Borchers CH. 2010. Crosslinking combined with mass spectrometry for structural proteomics. *Mass Spectrom. Rev.* 29(6):862–76
27. Pierson NA, Chen L, Valentine SJ, Russell DH, Clemmer DE. 2011. Number of solution states of bradykinin from ion mobility and mass spectrometry measurements. *J. Am. Chem. Soc.* 133(35):13810–13
28. Herzog F, Kahraman A, Boehringer D, Mak R, Bracher A, et al. 2012. Structural probing of a protein phosphatase 2A network by chemical cross-linking and mass spectrometry. *Science* 337(6100):1348–52
29. Smith LP, Parkins WE, Forrester AT. 1947. On the separation of isotopes in quantity by electromagnetic means. *Phys. Rev.* 72(11):989–1002
30. Cooks RG, Jo SC, Green J. 2004. Collisions of organic ions at surfaces. *Appl. Surf. Sci.* 231–32:13–21
31. Johnson GE, Hu Q, Laskin J. 2011. Soft landing of complex molecules on surfaces. *Annu. Rev. Anal. Chem.* 4:83–104
32. Cyriac J, Pradeep T, Kang H, Souda R, Cooks RG. 2012. Low-energy ionic collisions at molecular solids. *Chem. Rev.* 112:5356–411
33. Verbeck G, Hoffmann W, Walton B. 2012. Soft-landing preparative mass spectrometry. *Analyst* 137(19):4393–407
34. Johnson GE, Gunaratne D, Laskin J. 2015. Soft- and reactive landing of ions onto surfaces: concepts and applications. *Mass Spectrom. Rev.* 2015:1–41
35. Kahle S, Deng Z, Malinowski N, Tonnoir C, Forment-Aliaga A, et al. 2012. The quantum magnetism of individual manganese-12-acetate molecular magnets anchored at surfaces. *Nano Lett.* 12:518–21

36. Kley CS, Dette C, Rinke G, Patrick CE, Cechal J, et al. 2014. Atomic-scale observation of multiconformational binding and energy level alignment of ruthenium-based photosensitizers on TiO_2 anatase. *Nano Lett.* 14:563–69
37. Grill V, Shen J, Evans C, Cooks RG. 2001. Collisions of ions with surfaces at chemically relevant energies: instrumentation and phenomena. *Rev. Sci. Instrum.* 72(8):3149–79
38. Alvarez J, Cooks RG, Barlow SE, Gaspar DJ, Futrell JH, Laskin J. 2005. Preparation and in situ characterization of surfaces using soft landing in a Fourier transform ion cyclotron resonance mass spectrometer. *Anal. Chem.* 77(11):3452–60
39. Rauschenbach S, Stadler FL, Lunedei E, Malinowski N, Koltsov S, et al. 2006. Electrospray ion beam deposition of clusters and biomolecules. *Small* 2:540–47
40. Volny M, Turecek F. 2006. High efficiency in soft landing of biomolecular ions on a plasma-treated metal surface: Are double-digit yields possible? *J. Mass Spectrom.* 41(1):124–26
41. Swarbrick JC, Taylor JB, O'Shea JN. 2006. Electrospray deposition in vacuum. *Appl. Surf. Sci.* 252(15):5622–26
42. O'Sullivan MC, Sprafke JK, Kondratuk DV, Rinfray C, Claridge TDW, et al. 2011. Vernier templating and synthesis of a 12-porphyrin nano-ring. *Nature* 469:72–75
43. Saywell A, Magnano G, Satterley CJ, Perdigão LMA, Britton AJ, et al. 2010. Self-assembled aggregates formed by single-molecule magnets on a gold surface. *Nat. Commun.* 1:75
44. O'Shea JN, Taylor JB, Swarbrick JC, Magnano G, Mayor LC, Schulte K. 2007. Electrospray deposition of carbon nanotubes in vacuum. *Nanotechnology* 18(3):035707
45. Kelly RT, Tolmachev AV, Page JS, Tang K, Smith RD. 2010. The ion funnel: theory, implementations, and applications. *Mass Spectrom. Rev.* 29:294
46. Pauly M, Sroka M, Reiss J, Rinke G, Albarghash A, Vogelgesang R, et al. 2014. A hydrodynamically optimized nano-electrospray ionization source and vacuum interface. *Analyst* 139:1856–67
47. Gunaratne KDD, Prabhakaran V, Ibrahim YM, Norheim RV, Johnson GE, Laskin J. 2015. Design and performance of a high-flux electrospray ionization source for ion soft landing. *Analyst* 140(9):2957–63
48. Lin B, Sunner J. 1994. Ion transport by viscous gas flow through capillaries. *J. Am. Soc. Mass Spectrom.* 5:873–85
49. Page JS, Marginean I, Baker ES, Kelly RT, Tang K, Smith RD. 2009. Biases in ion transmission through an electrospray ionization–mass spectrometry capillary inlet. *J. Am. Soc. Mass Spectrom.* 20(12):2265–72
50. Schneider BB, Javaheri H, Covey TR. 2006. Ion sampling effects under conditions of total solvent consumption. *Rapid Commun. Mass Spectrom.* 20:1538–44
51. Page JS, Tang K, Kelly RT, Smith RD. 2008. Subambient pressure ionization with nanoelectrospray source and interface for improved sensitivity in mass spectrometry. *Anal. Chem.* 80(5):1800–5
52. Konermann L, Ahadi E, Rodriguez AD, Vahidi S. 2013. Unraveling the mechanism of electrospray ionization. *Anal. Chem.* 85:2–9
53. Cox JT, Marginean I, Smith RD, Tang K. 2015. On the ionization and ion transmission efficiencies of different ESI-MS interfaces. *J. Am. Soc. Mass Spectrom.* 26(1):55–62
54. Brune H. 1998. Microscopic view of epitaxial metal growth: nucleation and aggregation. *Surface Sci. Rep.* 31(4–6):121–229
55. Barth JV. 2007. Molecular architectonic on metal surfaces. *Annu. Rev. Phys. Chem.* 58:375–407
56. Barth JV. 2000. Transport of adsorbates at metal surfaces: from thermal migration to hot precursors. *Surface Sci. Rep.* 40(3):75–149
57. Weckesser J, Barth JV, Kern K. 2001. Mobility and bonding transition of C_{60} on Pd(110). *Phys. Rev. B* 64(16):161403
58. Schunack M, Linderoth TR, Rosei F, Lægsgaard E, Stensgaard I, Besenbacher F. 2002. Long jumps in the surface diffusion of large molecules. *Phys. Rev. Lett.* 88(15):156102
59. Miller SA, Luo H, Pachuta SJ, Cooks RG. 1997. Soft-landing of polyatomic ions at fluorinated self-assembled monolayer surfaces. *Science* 275(5305):1447–50
60. Laskin J, Wang P, Hadjar O, Futrell JH, Alvarez J, Cooks RG. 2007. Charge retention by peptide ions soft-landed onto self-assembled monolayer surfaces. *Int. J. Mass Spectrom.* 265:237–43
61. Johnson GE, Priest T, Laskin J. 2011. Charge retention by gold clusters on surfaces prepared using soft landing of mass selected ions. *ACS Nano* 6(1):573–82

62. Gologan B, Green JR, Alvarez J, Laskin J, Cooks RG. 2005. Ion/surface reactions and ion soft-landing. *Phys. Chem. Chem. Phys.* 7(7):1490–500
63. Rauschenbach S, Vogelgesang R, Malinowski N, Gerlach JW, Benyoucef M, et al. 2009. Electrospray ion beam deposition: soft-landing and fragmentation of functional molecules at solid surfaces. *ACS Nano* 3:2901–10
64. Dubey G, Urcuyo R, Abb S, Rinke G, Burghard M, et al. 2014. Chemical modification of graphene via hyperthermal molecular reaction. *J. Am. Chem. Soc.* 136:13482–85
65. Rinke G, Rauschenbach S, Harnau L, Albarghash A, Pauly M, Kern K. 2014. Active control of protein conformation on metals by hyperthermal surface interaction. *Nanoletters* 14:5609–15
66. Räder HJ, Rouhanipour A, Talarico AM, Palermo V, Samori P, Müllen K. 2006. Processing of giant graphene molecules by soft-landing mass spectrometry. *Nat. Mater.* 5(4):276–80
67. Rauschenbach S, Rinke G, Malinowski N, Weitz RT, Dinnebier R, et al. 2012. Crystalline inverted membranes grown on surfaces by electrospray ion beam deposition in vacuum. *Adv. Mater.* 24:2761–67
68. Hauptmann N, Hamann C, Tang H, Berndt R. 2013. Switching and charging of a ruthenium dye on Ag(111). *Phys. Chem. Chem. Phys.* 15:10326–30
69. Hauptmann N, Scheil K, Gopakumar TG, Otte FL, Schütt C, et al. 2013. Surface control of alkyl chain conformations and 2D chiral amplification. *J. Am. Chem. Soc.* 135:8814–17
70. Rinke G, Rauschenbach S, Schrettl S, Hoheisel TN, Blohm J, et al. 2015. Soft-landing electrospray ion beam deposition of sensitive oligoynes on surfaces in vacuum. *Int. J. Mass. Spectrom.* 377:228–34
71. Abb S, Harnau L, Gutzler R, Rauschenbach S, Kern K. 2016. Two-dimensional honeycomb network through sequence-controlled self-assembly of oligopeptides. *Nat. Commun.* 7:10335
72. Böttcher A, Weis P, Jester S-S, Löffler D, Bihlmeier A, et al. 2005. Solid C_{58} films. *Phys. Chem. Chem. Phys.* 7:2816–20
73. Thontasen N, Levita G, Malinowski N, Deng Z, Rauschenbach S, Kern K. 2010. Grafting crown ether alkali host–guest complexes at surfaces by electrospray ion beam deposition. *J. Phys. Chem. C* 114:17768–72
74. Gunaratne KDD, Johnson GE, Andersen A, Dan Du WZ, Prabhakaran V, et al. 2014. Controlling the charge state and redox properties of supported polyoxometalates via soft landing of mass-selected ions. *J. Phys. Chem. C* 118:27611–22
75. Witten TA Jr, Sander LM. 1981. Diffusion-limited aggregation, a kinetic critical phenomenon. *Phys. Rev. Lett.* 47(19):1400
76. Dil H, Lobo-Checa J, Laskowski R, Blaha P, Berner S, et al. 2008. Surface trapping of atoms and molecules with dipole rings. *Science* 319(5871):1824–26
77. Grimley TB. 1967. The indirect interaction between atoms or molecules adsorbed on metals. *Proc. Phys. Soc.* 90:751
78. Lau KH, Kohn W. 1978. Indirect long-range oscillatory interaction between adsorbed atoms. *Surf. Sci.* 75:69
79. Silly F, Pivetta M, Ternes M, Patthey F, Pelz JP, Schneider WD. 2004. Creation of an atomic superlattice by immersing metallic adatoms in a two-dimensional electron sea. *Phys. Rev. Lett.* 92:016101
80. von Hofe T, Kröger J, Berndt R. 2006. Adsorption geometry of Cu(111)-Cs studied by scanning tunneling microscopy. *Phys. Rev. B* 73:245434
81. Ziegler M, Kröger J, Berndt R, Filinov A, Bonitz M. 2008. Scanning tunneling microscopy and kinetic Monte Carlo investigation of cesium superlattices on Ag(111). *Phys. Rev. B* 78:245427
82. Yokoyama T, Takahashi T, Shinozaki K. 2007. Quantitative analysis of long-range interactions between adsorbed dipolar molecules on Cu(111). *Phys. Rev. Lett.* 98:206102
83. Fernandez-Torrente I, Monturet S, Franke KJ, Fraxedas J, Lorente N, Pascual JI. 2007. Long-range repulsive interaction between molecules on a metal surface induced by charge transfer. *Phys. Rev. Lett.* 99:176103
84. Ternes M, Weber C, Pivetta M, Patthey F, Pelz JP, et al. 2004. Scanning-tunneling spectroscopy of surface-state electrons scattered by a slightly disordered two-dimensional dilute "solid": Ce on Ag(111). *Phys. Rev. Lett.* 93:146805
85. Negulyaev NN, Stepanyuk VS, Niebergall L, Bruno P, Pivetta M, et al. 2009. Melting of two-dimensional adatom superlattices stabilized by long-range electronic interactions. *Phys. Rev. Lett.* 102:246102

86. Ternes M, Pivetta M, Patthey F, Schneider WD. 2010. Creation, electronic properties, disorder, and melting of two-dimensional surface-state-mediated adatom superlattices. *Prog. Surf. Sci.* 85:1
87. Wagner C, Green MFB, Leinen P, Deilmann T, Krüger P, et al. 2015. Scanning quantum dot microscopy. *Phys. Rev. Lett.* 115:026101
88. Mohn F, Gross L, Moll N, Meyer G. 2012. Imaging the charge distribution within a single molecule. *Nat. Nanotechnol.* 7:227–31
89. Wysocki VH, Joyce KE, Jones CM, Beardsley RL. 2008. Surface-induced dissociation of small molecules, peptides, and non-covalent protein complexes. *J. Am. Soc. Mass Spectrom.* 19:190–208
90. Wang P, Hadjar O, Laskin J. 2007. Covalent immobilization of peptides on self-assembled monolayer surfaces using soft-landing of mass-selected ions. *J. Am. Chem. Soc.* 129(28):8682–83
91. Wang P, Hadjar O, Gassman PL, Laskin J. 2008. Reactive landing of peptide ions on self-assembled monolayer surfaces: an alternative approach for covalent immobilization of peptides on surfaces. *Phys. Chem. Chem. Phys.* 10(11):1512–22
92. Pepi F, Tata A, Garzoli S, Giacomello P, Ragno R, et al. 2011. Chemically modified multiwalled carbon nanotubes electrodes with ferrocene derivatives through reactive landing. *J. Phys. Chem. C* 115(11):4863–71
93. Krasheninnikov AV, Nordlund K. 2010. Ion and electron irradiation-induced effects in nanostructured materials. *J. Appl. Phys.* 107:071301
94. Wilhelm RA, Gruber E, Ritter R, Heller R, Facsko S, Aumayr F. 2014. Charge exchange and energy loss of slow highly charged ions in 1 nm thick carbon nanomembranes. *Phys. Rev. Lett.* 112(15):153201
95. Ouyang Z, Takats Z, Blake TA, Gologan B, Guymon AJ, et al. 2003. Preparing protein microarrays by soft-landing of mass-selected ions. *Science* 301(5638):1351–54
96. Wang P, Laskin J. 2008. Helical peptide arrays on self-assembled monolayer surfaces through soft and reactive landing of mass-selected ions. *Angew Chem. Int. Ed.* 47:6678–80
97. Luo H, Miller SA, Cooks RG, Pachuta SJ. 1998. Soft landing of polyatomic ions for selective modification of fluorinated self-assembled monolayer surfaces. *Int. J. Mass Spectrom.* 174(1–3):193–217
98. Gologan B, Takats Z, Alvarez J, Wiseman JM, Talaty N, et al. 2004. Ion soft-landing into liquids: protein identification, separation, and purification with retention of biological activity. *J. Am. Soc. Mass Spectrom.* 15(12):1874–84
99. Clemmer DE, Hudgins RR, Jarrold MF. 1995. Naked protein conformations – cytochrome *c* in the gas-phase. *J. Am. Chem. Soc.* 117:10141–42
100. Shelimov KB, Clemmer DE, Hudgins RR, Jarrold MF. 1997. Protein structure in vacuo: gas-phase conformations of BPTI and cytochrome *c*. *J. Am. Chem. Soc.* 119:2240–48
101. Hoaglund-Hyzer CS, Counterman AE, Clemmer DE. 1999. Anhydrous protein ions. *Chem. Rev.* 99(10):3037–80
102. Wyttenbach T, Pierson NA, Clemmer DE, Bowers MT. 2014. Ion mobility analysis of molecular dynamics. *Annu. Rev. Phys. Chem.* 65:175–96
103. Deng Z, Thontasen N, Malinowski N, Rinke G, Harnau L, et al. 2012. A close look at proteins: submolecular resolution of two- and three-dimensionally folded cytochrome *c* at surfaces. *Nano Lett.* 12:2452–58
104. Gross L, Mohn F, Moll N, Schuler B, Criado A, et al. 2012. Bond-order discrimination by atomic force microscopy. *Science* 337:1326
105. Weiss C, Wagner C, Kleimann C, Rohlfing M, Tautz FS, Temirov R. 2010. Imaging Pauli repulsion in scanning tunneling microscopy. *Phys. Rev. Lett.* 105:086103
106. Hapala P, Temirov R, Tautz FS, Jelínek P. 2014. Origin of high-resolution IETS-STM images of organic molecules with functionalized tips. *Phys. Rev. Lett.* 113:226101
107. Longchamp J-N, Latychevskaia T, Escher C, Fink H-W. 2013. Graphene unit cell imaging by holographic coherent diffraction. *Phys. Rev. Lett.* 110(25):255501
108. Chapman HN, Fromme P, Barty A, White TA, Kirian RA, et al. 2011. Femtosecond X-ray protein nanocrystallography. *Nature* 470(7332):73–77
109. Lutz J-F, Ouchi M, Liu DR, Sawamoto M. 2013. Sequence-controlled polymers. *Science* 341(6146):1238149
110. Goodman CM, Choi S, Shandler S, DeGrado WF. 2007. Foldamers as versatile frameworks for the design and evolution of function. *Nat. Chem. Biol.* 3(5):252–62

111. Lingenfelder M, Tomba G, Costantini G, Colombi Ciacchi L, De Vita A, Kern K. 2007. Tracking the chiral recognition of adsorbed dipeptides at the single-molecule level. *Angew. Chem. Int. Ed.* 46(24):4492–95
112. Rauschenbach S, Rinke G, Gutzler R, Abb S, Albargash A, et al. 2016. Molecular nanostructures through two-dimensional folding of polypeptides at surfaces. Submitted
113. Wei T, Carignano MA, Szleifer I. 2011. Lysozyme adsorption on polyethylene surfaces: Why are long simulations needed? *Langmuir* 27(19):12074–81
114. Zhong D, Franke J-H, Podiyanachari SK, Blömker T, Zhang H, et al. 2011. Linear alkane polymerization on a gold surface. *Science* 334:213–16
115. Tanaka H, Kawai T. 2009. Partial sequencing of a single DNA molecule with a scanning tunneling microscope. *Nat. Nanotechnol.* 4:518–22
116. Wagner C, Temirov R. 2015. Tunnelling junctions with additional degrees of freedom: an extended toolbox of scanning probe microscopy. *Prog. Surf. Sci.* 90:194
117. Gross L, Mohn F, Liljeroth P, Repp J, Giessibl FJ, Meyer G. 2009. Measuring the charge state of an adatom with noncontact atomic force microscopy. *Science* 324:1428–31
118. Tersoff J, Hamann DR. 1985. Theory of the scanning tunneling microscope. *Phys. Rev. B* 31:805–13
119. Lang ND. 1986. Spectroscopy of single atoms in the scanning tunneling microscope. *Phys. Rev. B* 34:5947–50
120. Stipe BC, Rezaei MA, Ho W. 1998. Single-molecule vibrational spectroscopy and microscopy. *Science* 280:1732–35
121. Heinrich AJ, Gupta JA, Lutz CP, Eigler DM. 2004. Single-atom spin-flip spectroscopy. *Science* 306:466–69
122. Heinrich AJ, Lutz CP, Gupta JA, Eigler DM. 2002. Molecule cascades. *Science* 298:1381–87
123. Natterer FD, Patthey F, Brune H. 2013. Distinction of nuclear spin states with the scanning tunneling microscope. *Phys. Rev. Lett.* 111:175303
124. Vitali L, Levita G, Ohmann R, Comisso A, De Vita A, Kern K. 2010. Portrait of the potential barrier at metal–organic nanocontacts. *Nat. Mater.* 9:320–23
125. Loth S, Etzkorn M, Lutz CP, Eigler DM, Heinrich AJ. 2010. Measurement of fast electron spin relaxation times with atomic resolution. *Science* 329:1628–30
126. Grosse C, Etzkorn M, Kuhnke K, Loth S, Kern K. 2013. Quantitative mapping of fast voltage pulses in tunnel junctions by plasmonic luminescence. *Appl. Phys. Lett.* 103:183108
127. Yan S, Choi D-J, Burgess JAJ, Rolf-Pissarczyk S, Loth S. 2015. Control of quantum magnets by atomic exchange bias. *Nat. Nanotechnol.* 10:40–45
128. Hölscher H, Langkat SM, Schwarz A, Wiesendanger R. 2002. Measurement of three-dimensional force fields with atomic resolution using dynamic force spectroscopy. *Appl. Phys. Lett.* 81:4428
129. Hauptmann N, Hamann C, Tang H, Berndt R. 2013. Soft-landing electrospray deposition of the ruthenium dye N3 on Au(111). *J. Phys. Chem. C* 117:9734–38
130. Kley CS, Dette C, Rinke G, Patrick CE, Čechal J, et al. 2014. Atomic-scale observation of multiconformational binding and energy level alignment of ruthenium-based photosensitizers on TiO_2 anatase. *Nano Lett.* 14:563–69
131. Sessoli R, Gatteschi D, Caneschi A, Novak MA. 1993. Magnetic bistability in a metal-ion cluster. *Nature* 365:141–43
132. Mannini M, Pineider F, Sainctavit P, Cartier dit Moulin C, Arrio M-A, Cornia A. 2009. XMCD of a single layer of single molecule magnets. *Eur. Phys. J.* 169(1):167–73
133. Mannini M, Sainctavit P, Sessoli R, Cartier dit Moulin C, Pineider F, et al. 2008. XAS and XMCD investigation of Mn_{12} monolayers on gold. *Chem. Eur. J.* 14:7530–35
134. Ternes M. 2015. Spin excitations and correlations in scanning tunneling spectroscopy. *New J. Phys.* 17:063016
135. Nie Z, Li G, Goodwin MP, Gao L, Cyriac J, Cooks RG. 2009. In situ SIMS analysis and reactions of surfaces prepared by soft landing of mass-selected cations and anions using an ion trap mass spectrometer. *J. Am. Soc. Mass Spectrom.* 20:949–56
136. Cyriac J, Wleklinski M, Li G, Liang Gao, Cooks RG. 2012. In situ Raman spectroscopy of surfaces modified by ion soft landing. *Analyst* 137(6):1363–69

137. Chen Y, Deng K, Qiu X, Wang C. 2013. Visualizing cyclic peptide hydration at the single-molecule level. *Sci. Rep.* 3:2461
138. Li A, Luo Q, Park S-J, Cooks RG. 2014. Synthesis and catalytic reactions of nanoparticles formed by electrospray ionization of coinage metals. *Angew Chem.* 126:3211–14
139. Laskin j, Wang P, Hadjar O. 2010. Soft-landing of CoIII(salen)+ and NnIII(salen)+ on self-assembled monolayer surfaces. *J. Phys. Chem. C* 114:5305–11
140. Hamann C, Woltmann R, Hong I-P, Hauptmann N, Karan S, Berndt R. 2011. Ultrahigh vacuum deposition of organic molecules by electrospray ionization. *Rev. Sci. Instr.* 82(3):033903
141. Mayor LC, Saywell A, Magnano G, Satterley CJ, Schnadt J, O'Shea JN. 2009. Adsorption of a Ru(ii) dye complex on the Au(111) surface: photoemission and scanning tunneling microscopy. *J. Chem. Phys.* 130:164704
142. Assig M, Etzkorn M, Enders A, Stiepany W, Ast CR, Kern K. 2013. A 10 mK scanning tunneling microscope operating in ultra-high vacuum and high magnetic fields. *Rev. Sci. Instrum.* 84(3):033903